

Influence of Carrier Gas on Particle Size in Chemical Vapor Synthesis of Nanocrystalline Iron Oxide

A. Kompch¹⁾, W. Jin¹⁾, I.-K. Lee¹⁾, M. Winterer¹⁾

¹⁾ Nanoparticle Process Technology, Universität Duisburg-Essen, Germany

ABSTRACT

The effect of the carrier gas on the characteristics of iron oxide particles in a hot-wall flow reactor was investigated. Iron oxide particles in the nanometer range were prepared from iron pentacarbonyl and oxygen as precursors using CO₂, N₂, Ar and He as carrier gases. Rietveld refinement of x-ray diffraction patterns revealed a phase mixture of maghemite and hematite with particle sizes decreasing with the heat capacity of the carrier gas. Particle size measurements from TEM images and surface area measurements by gas adsorption support this result.

1 INTRODUCTION

Chemical vapor synthesis is a modified CVD process where the conditions are adapted to form particles instead of thin films. Here we report on the synthesis and characterization of nanocrystalline iron oxide particles in a hot wall flow reactor from iron pentacarbonyl as precursor [1]. Special attention is paid to investigate the effect of different carrier gases used for the process. Nanocrystalline iron oxide particles are widely used as catalysts in Super-Claus-processes to obtain elementary sulfide from refinery of crude oil [2]. They can also be used as catalysts in the synthesis of multiwalled carbon nanotubes with controllable diameter [3] or with a special outer hydrophilic and an inner hydrophobic region for the extraction of soluble organic compounds from water by application of an external magnetic field [4]. Due to their chemical stability under normal laboratory conditions unlike pure metals or nitrides they are ideal to investigate the effect of process parameters on their properties.

2 EXPERIMENTAL PROCEDURE

Iron oxide nanoparticles were synthesized in a hot wall flow reactor consisting of three concentric tubes in a furnace (Fig. 1). The precursor was "bubbled" (CH2), diluted with inert carrier gas (CH1) and delivered to the reaction zone by a nozzle (inner tube) that reached just to the beginning of the heated zone. Oxygen (CH4) mixed with carrier gas (CH5) was supplied to the reaction tube (middle tube) from the top of the reactor. The gas stream in the outer shell tube (CH7) mixes with the particle gas flow at the end of the reactor inside the sampling chamber for further dilution and prevention of deposition and agglomeration. Gas flows were controlled by mass flow controllers and were set as shown in table 1. For comparison with previous experiments [1, 5, 6] the

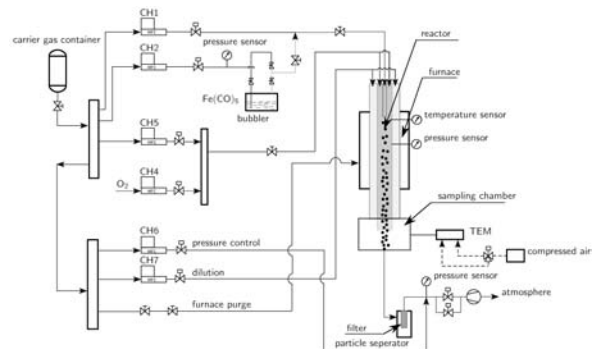


Figure 1: Experimental setup (hot wall flow reactor, gas and precursor delivery system, particle separator) for the synthesis of iron oxide from liquid iron pentacarbonyl precursor

gas flow in the reaction tube was set to a total of 3 slm and 7 slm in the outer shell tube. All experiments were carried out at a pressure of 200 mbar inside the reactor and at a temperature of 800 °C with Nitrogen as carrier gas and at 700 °C with Nitrogen, Argon, Helium and Carbon Dioxide as carrier gases. The oxygen flow (CH4) was set to approximately five times the needed amount for the complete conversion of Fe(CO)₅ to Fe₂O₃ and CO₂ as calculated in advance with the bubbler equation (see equation 1).

Table 1: Process parameters and mass of collected particles

| Experiment [Fe _x O _y] | AK2 | AK3 | AK6 | AK9 | AK10 | AK14 |
|--|----------------|----------------|----------------|--------|--------|-----------------|
| Pressure [mbar] | 200 | 200 | 200 | 200 | 200 | 200 |
| Temperature [°C] | 700 | 800 | 700 | 700 | 700 | 700 |
| Carrier gas | N ₂ | N ₂ | N ₂ | Ar | He | CO ₂ |
| CH1 [sccm] carrier gas | | | 625 | | | |
| CH2 [sccm] carrier gas (bubbler) | | | 25 | | | |
| CH4 [sccm] oxygen | | | 350 | | | |
| CH5 [sccm] carrier gas | | | 2000 | | | |
| CH6 [sccm] pressure control | | | 6000 - 8000 | | | |
| CH7 [sccm] carrier gas (dilution) | | | 7000 | | | |
| Collected powder [g] | 0.3990 | 1.1389 | 0.8500 | 0.6991 | 0.6293 | 45.4100 |
| Actual precursor used [g] | 0.8 | | 1.1 | 3.1 | 3.3 | 143.2 |
| Actual O ₂ -excess | 36.10 | | 24.69 | 9.79 | 8.14 | 0.1 |
| Yield [%] | | | | 55 | 47 | 78 |
| Duration [min] | 63 | 95 | 60 | 71 | 64 | 30 |
| Deposition on reactorwall [yes/no] | no | no | no | no | yes | yes |
| Bubbler thermostat [T in °C] | not used | not used | 32.00 | 32.00 | 32.00 | 32.00 |

$$\dot{m}_{prec} = \frac{p_{prec}}{p_{bubbler} - p_{prec}} \frac{M_{prec}}{M_{carrier}} \dot{m}_{carrier} \quad (1)$$

The partial pressure of the precursor P_{prec} in the bubbler is assumed to be equal to the precursor vapour pressure at the temperature of the bubbler thermostat (54.44 mbar at 32 °C). The pressure inside the bubbler $p_{bubbler}$ is detected by another pressure sensor. The molar masses of the precursor and carrier gas are M_{prec} and $M_{carrier}$ respectively. The mass flow of carrier gas as set in table 1 (CH2) is $m_{carrier}$. Pressure control (CH6) was realized by a vacuum pump and means of an additional controlled gas flow after the particle collector. The sampling chamber was equipped with an in-situ TEM sampling mechanism that uses a pressure driven piston to deliver a TEM-grid to the reactor axis for 138 ms. Particles were collected and characterized by X-ray diffraction using a Philips PW 1729 with Cu K_{α} radiation and a diffracted beam monochromator. The range was from 15 ° to 125 ° 2 θ with a step size of 0.05 ° 2 θ and integration time was 100 s. Rietveld refinement using the program FullProf [7] and WinPLOTR [8] was employed to identify the phases and unit cell size. Crystallite size was calculated using a FullProf subroutine [9]. Nitrogen adsorption measurements were performed utilizing a Quantachrome Nova 1000 and Autosorb-1-C at 77 K after heating the samples at 120 °C for 12 hours under vacuum to remove any adsorbants especially water from the particle surface. Assuming monodisperse particles without pores the mean particle diameter d can be calculated from the specific surface area S using the bulk density of α -Fe₂O₃ $\rho=5.3$ g/cm³ (see equation 2).

$$d = \frac{6}{\rho S} \quad (2)$$

3 RESULTS

Experiments took between 30 and 95 minutes and yielded a reddish powder. The amount of particles collected was between 0.39 g and 45.4 g (see Table 1). The yield was calculated assuming a complete conversion of Fe(CO)₅ to Fe₂O₃. The synthesis of nanoparticles took place at rates of about 0.5 g/h with a yield of approximately 50 % or more. For all experiments the condition of ample oxygen excess was maintained except for AK14. Here the particles were dark red-brown in colour and originally probably a mixture of all kinds of iron and iron oxides. The plentiful consumption of precursor in this experiment can only be explained by major pressure variations inside the bubbler.

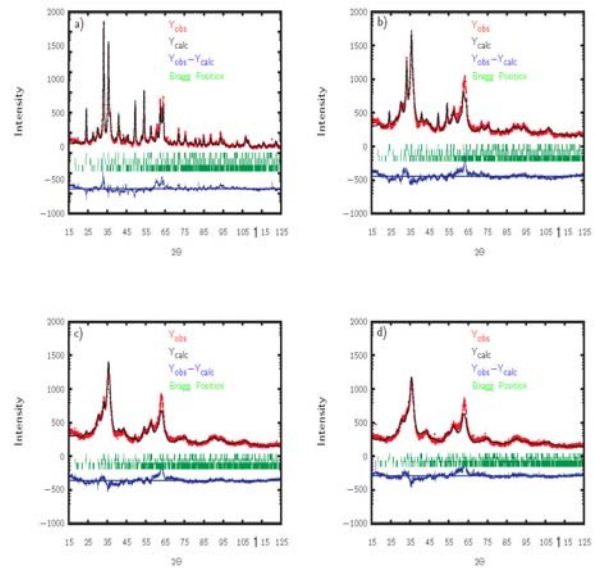


Figure 2: X-ray diffractogram and Rietveld refinement of experiments a) AK3 b) AK6 c) AK9 d) AK10 using a phase mixture of α -, γ -, ϵ -Fe₂O₃

3.1 Rietveld refinement

Rietveld refinement was carried out using a phase mixture α -, γ - and ϵ -Fe₂O₃ since a preliminary analysis (using the program genfit [10]) of the x-ray diffractograms by comparison with the most intense reflexes from α -Fe₂O₃ (104, 110) and γ -Fe₂O₃ (311) between 31 ° and 39 ° 2 θ revealed a reflex at approximately 37 ° 2 θ that could not be attributed to either iron oxide phase. Starting parameters for α -Fe₂O₃ were taken from [11] for γ -Fe₂O₃ from [12] and for ϵ -Fe₂O₃ from [13]. Tables 2 and 3 show the refined parameters and their starting values. Along with the temperature change from 800 °C to 700 °C the ratio of α -Fe₂O₃ to γ -Fe₂O₃ in the mixture

Table 2: Final and starting parameters for rietveld refinement of x-ray diffractograms from experiments AK3 and AK6

| Parameter | Literature | Fe ₂ O ₃ AK3 | σ | Fe ₂ O ₃ AK6 | σ |
|--|-------------------------|------------------------------------|-----------|------------------------------------|-----------|
| Phase 1 α-Fe₂O₃ | | | | | |
| | R-3C(167) | | | | |
| Scale Factor | | 0.000525 | 0.0000076 | 0.000184 | 0.0000068 |
| Fraction | | 47% | 1.04 | 15.5% | 0.66 |
| a,b | 5.0347(4) Å | 5.0385 Å | 0.00033 | 5.039 Å | 0.001 |
| c | 13.7473(15) Å | 13.762 Å | 0.0013 | 13.742 Å | 0.0041 |
| Y | | 0.336 | 0.0075 | 0.52 | 0.026 |
| Crystal Size | | 16.7 nm | 0.58 | 10.7 nm | 0.78 |
| Bragg-R | | 13.3 | | 13.7 | |
| Phase 2 γ-Fe₂O₃ | | | | | |
| | P4 ₃ 32(212) | | | | |
| Scale Factor | | 0.000105 | 0.0000039 | 0.000234 | 0.0000050 |
| Fraction | | 32% | 1.29 | 67% | 2.00 |
| a,b,c | 8.3457 Å | 8.329 Å | 0.0025 | 8.349 Å | 0.0021 |
| Y | | 1.68 | 0.076 | 2.32 | 0.052 |
| Crystal Size | | 3.3 nm | 0.23 | 2.42 nm | 0.08 |
| Bragg-R | | 14.9 | | 10.4 | |
| Phase 3 ϵ-Fe₂O₃ | | | | | |
| | PNA2 ₁ (33) | | | | |
| Scale Factor | | 0.000128 | 0.0000059 | 0.000112 | 0.0000093 |
| Fraction | | 21% | 1.06 | 18% | 1.51 |
| a | 5.095(1) Å | 5.101 Å | 0.0018 | 5.102 Å | 0.0065 |
| b | 8.789(2) Å | 8.786 Å | 0.0037 | 8.85 Å | 0.012 |
| c | 9.437(3) Å | 9.495 Å | 0.0030 | 9.469 Å | 0.0091 |
| Y | | 0.50 | 0.032 | 1.2 | 0.11 |
| Crystal Size | | 11.4 nm | 1.08 | 4.5 nm | 0.57 |
| Bragg-R | | 22.6 | | 15.0 | |
| Global | | | | | |
| 2 θ -Offset | | 0.247 | 0.0063 | 0.166 | 0.0018 |
| R _{wp} | | 25.8 | | 21 | |
| R _{exp} | | 9.42 | | 9.58 | |

Table 3: Final and starting parameters for Rietveld refinement of x-ray diffractograms from experiments AK9 and AK10

| Parameter | Literature | Fe ₂ O ₃ AK9 | σ | Fe ₂ O ₃ AK10 | σ |
|--|-------------------------|------------------------------------|-----------|-------------------------------------|-----------|
| Phase 1 | | | | | |
| α -Fe ₂ O ₃ | R-3C(167) | | | | |
| Scale Factor | | 0.000073 | 0.0000072 | 0.000025 | 0.0000084 |
| Fraction | | 6.6% | 0.67 | 2.4% | 0.8 |
| a,b | 5.0347(4) Å | 5.042 Å | 0.003 | 5.08 Å | 0.011 |
| c | 13.7473(15) Å | 13.70 Å | 0.011 | 13.39 Å | 0.041 |
| Y | | 0.74 | 0.086 | 0.9 | 0.35 |
| Crystal Size | | 7.6 nm | 1.26 | 6.0 nm | 2.58 |
| Bragg-R | | 12 | | 11.1 | |
| Phase 2 | | | | | |
| γ -Fe ₂ O ₃ | P4 ₃ 32(212) | | | | |
| Scale Factor | | 0.000243 | 0.0000049 | 0.000242 | 0.0000051 |
| Fraction | | 75% | 2.27 | 79% | 2.53 |
| a,b,c | 8.3457 Å | 8.34 Å | 0.0028 | 8.341 Å | 0.0035 |
| Y | | 2.36 | 0.048 | 2.60 | 0.052 |
| Crystal Size | | 2.38 nm | 0.07 | 2.16 nm | 0.07 |
| Bragg-R | | 10.2 | | 10.5 | |
| Phase 3 | | | | | |
| ϵ -Fe ₂ O ₃ | PNA2 ₁ (33) | | | | |
| Scale Factor | | 0.000108 | 0.0000092 | 0.000108 | 0.0000091 |
| Fraction | | 19% | 1.63 | 19% | 1.67 |
| a | 5.095(1) Å | 5.227 Å | 0.0055 | 5.132 Å | 0.0059 |
| b | 8.789(2) Å | 9.24 Å | 0.011 | 9.22 Å | 0.010 |
| c | 9.437(3) Å | 8.848 Å | 0.0092 | 8.88 Å | 0.011 |
| Y | | 1.4 | 0.15 | 1.4 | 0.15 |
| Crystal Size | | 4.1 nm | 0.64 | 4.0 nm | 0.61 |
| Bragg-R | | 12.4 | | 12.5 | |
| Global | | | | | |
| 2 θ -Offset | | 0.07 | 0.031 | 0.24 | 0.039 |
| R _{wp} | | 19.7 | | 20.1 | |
| R _{exp} | | 10.13 | | 10.35 | |

is switched from α -Fe₂O₃ as the major fraction of the powder to γ -Fe₂O₃. Oxide phases containing Fe²⁺ or Fe⁴⁺ can be excluded as Fe₂O₃ is the favored phase at temperatures below 1000 °C in the presence of oxygen excess. This is consistent with α -Fe₂O₃ being the thermodynamically most stable phase of the iron oxides [14] and the findings in [1] that revealed phase mixtures of α -Fe₂O₃ and γ -Fe₂O₃ up to a synthesis temperature of 900 °C. It is interesting to note that in all experiments γ -Fe₂O₃-particles were the smallest with a size of roughly 2 nm. ϵ -Fe₂O₃ is the "youngest" of iron oxides as its structure has only recently been completely described [13]. Its structure has numerous intermediate features of α -Fe₂O₃ and γ -Fe₂O₃ and has so far only been found as nanosized crystalline particles in mixtures with both. Further the transformation temperature of ϵ -Fe₂O₃ to α -Fe₂O₃ which falls in the range of 500 °C to 750 °C and of γ -Fe₂O₃ to α -Fe₂O₃ which starts at 400 °C is consistent with this characterization. However the fraction of ϵ -Fe₂O₃ remained surprisingly almost constant at both temperatures and with all carrier gases. Though no ϵ -Fe₂O₃ was found in previous experiments [1, 5, 6] it could be attributed to this being the first Rietveld analysis of synthesized nanoparticles from this reactor. The Rietveld refinement plot shows clearly that the missing reflexes can be explained by ϵ -Fe₂O₃ as part of the mixture.

3.2 Nitrogen adsorption measurements

Nitrogen adsorption measurements revealed particle sizes in the 8 to 16 nm range (see Table 4). Particles were larger at higher furnace temperatures which is consistent with previous results [1]. The size also increased depending on the carrier gas. Particles were larger with N₂ than with Ar or He. The result from CO₂ cannot be considered because the particles were synthesized under oxygen deficiency and must be of different chemical composition. However more experiments need to be performed and characterized to establish a definite dependence of the particle size

upon the properties of the carrier gas (e.g. molar weight or molar heat capacity, etc.).

3.3 TEM-Images

TEM micrographs (see Fig. 3) show samples synthesized at 800 °C with N₂ as carrier gas and samples synthesized at 700 °C with N₂ and Ar as carrier gas. The particles prepared at the lower temperature are smaller and linked together forming large agglomerates. This is not surprising as particles are transported to the filter with the hot gas stream and only slowly cool off after the experiment. Particles synthesized at 800 °C show also large agglomerates but most are already sintered with necks close to the same size as the particle diameter. From the scale it can be determined that the particles prepared at the higher temperature are also larger supporting the Rietveld, genfit and BET results (see Table 4).

3.4 Comparison of different particle size measurements

Table 4 compares the results from the different particle size measurements. Particle sizes determined for each experiment by BET, genfit and Rietveld refinement are in very good agreement and qualitatively supported by the TEM micrographs. Moreover it is confirmed that a higher synthesis temperature yields larger particles. The dependence of the particle size increasing with the molecular weight of the carrier gas as suggested in [15, 16] could not be confirmed. The data rather suggest that the particle size increases with the molar heat capacity of the carrier gas mixture. The molar heat capacity in table 4 is calculated using the mixture of carrier gas, oxygen and precursor concentration from table 1.

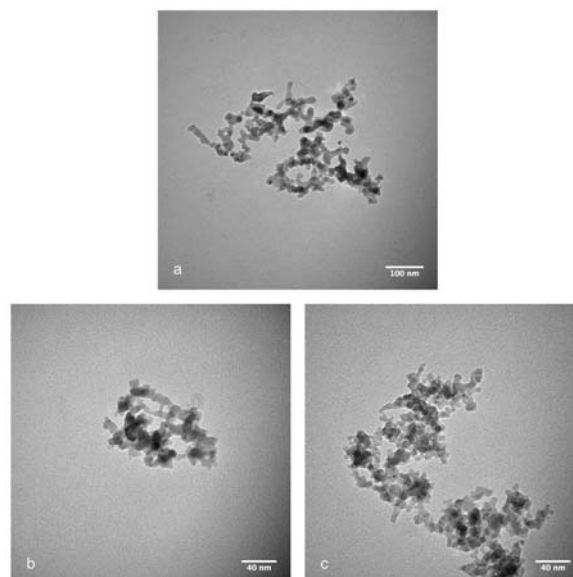


Figure 3: TEM micrographs of synthesized nanocrystalline Fe₂O₃ particles a) AK3; T=800 °C; 40k-magnification b) AK6; T=700 °C; 88k-magnification c) AK9; T=700 °C; 88k-magnification

This is the reason for the very high molar heat capacity in the CO₂ (c_p (CO₂ at 700 °C) = 53.98 J/(mol K)) experiment though it did not contribute to the analysis

due to the synthesis with oxygen deficiency. The molar heat capacity in all other experiments is very close to that of the pure carrier gas as the precursor concentration was much lower there. Finally it is clear that the size dependence upon the carrier gas is very limited compared to the effect of a higher or lower furnace temperature, reactor pressure or precursor concentration [1].

Table 4: Comparison of results from different particle size determinations

| Carrier Gas | | Ar | He | N ₂ | CO ₂ | N ₂ | |
|---------------------|-------------------------|-----------------|-----------|----------------|-----------------|----------------|-----------|
| Temperature | °C | 700 | 700 | 700 | 700 | 800 | |
| Molar Heat Capacity | $\frac{J}{mol \cdot K}$ | 22.72 | 22.78 | 32.78 | 79.20 | 33.55 | |
| Molar Weight | $\frac{g}{mol}$ | 39.95 | 4.0 | 28.01 | 44.01 | 28.01 | |
| BET- | | | | | | | |
| | spec. Surface Diameter | $\frac{m^2}{g}$ | 133.86 | 134.87 | 102.75 | 138.10 | 68.13 |
| Genfit | | d | σ | d | σ | d | σ |
| | α -Phase | nm | 10.9 2.86 | 7.4 1.02 | 18.3 3.04 | | 21.4 1.82 |
| Rietveld | | d | σ | d | σ | d | σ |
| | γ -Phase | nm | 5.0 0.88 | 4.8 0.24 | 7.3 0.99 | | 15.4 2.19 |
| Rietveld | | d | σ | d | σ | d | σ |
| | α -Phase | nm | 7.6 1.26 | 6.0 2.58 | 10.7 0.78 | | 16.7 0.58 |
| | γ -Phase | nm | 2.38 0.07 | 2.16 0.07 | 2.42 0.08 | | 3.3 0.23 |
| | ϵ -Phase | nm | 4.1 0.64 | 4.0 0.61 | 4.5 0.57 | | 11.4 1.08 |

ACKNOWLEDGEMENT:

The authors gratefully acknowledge the financial support of the German Research Foundation through the collaborative research center SFB 445. The authors thank also ThyssenKrupp AG for making available measurement time at their diffractometer. Additionally, we acknowledge the support by CeNIDE (Center for Nanointegration Duisburg-Essen)

REFERENCES:

- [1] Orthner, H. R.; Roth, P.: Formation of iron oxide powder in a hot-wall flow reactor Effect of process conditions on powder characteristics, Mater Chem Phys 2002, 78, p. 453-458
- [2] Kraan, A. M. v. d.: Fischer-Tropsch, hydrotreating and superClaus catalysts, Hyperfine Interact 111 (1998) p. 23-34
- [3] Kondo, D.; Sato, S.; Kawabata, A.; Awano, Y.: Diameter-Controlled Growth of Multi-Walled Carbon Nanotubes by Hot-Filament Chemical Vapor Deposition with Ferritin as a Catalyst on a Silicon Substrate, Jpn J Appl Phys 44 (2005) p. 5292-5295
- [4] Moeser, G. D.; Roach, K. A.; Green, W. H.; Laibinis, P. E.; Hatton, T. A.: Water-based Magnetic Fluids as Extractants for Synthetic Organic Compounds, Ind Eng Chem Res 41 (2002), p. 4739-4749
- [5] Knipping J.; Wiggers, H.; Kock, B. F.; Hülser, T.; Rellinghaus, B.; Roth, P.: Synthesis and characterization of nanowires formed by self-assembled iron particles, Nanotechnology 15 (2004) p. 1665-1670
- [6] Knipping J.; Kock, B. F.; Rellinghaus, B.; Roth, P.: Formation of Pure and Coated Iron Particles in a Hot Wall Flow Reactor, Proceedings of PARTEC, Nürnberg, Germany (2004)
- [7] Rodriguez-Carvajal, J.: FULLPROF: A Program for Rietveld Refinement and Pattern Matching Analysis. In:

Abstracts of the Satellite Meeting on Powder Diffraction of the XV Congress of the IUCr. Toulouse, France : IUCr, 1990, p. 127

[8] Rodriguez-Carvajal, J.; Roisnel, T.: WinPLOTR: a Windows tool for powder diffraction patterns analysis, Mat Sci Forum 378-381 (2001) p. 118-123

[9] Rodriguez-Carvajal, J.; Roisnel, T.: Line Broadening Analysis Using FullProf: Determination of Microstructural Properties. In: Andersson, Yvonne (Hrsg.) ; Mittemeijer, Eric J. (Hrsg.) ; Welzel, Udo (Hrsg.): Mat Sci Forum: Proceedings of the Eighth European Powder Diffraction Conference (EPDIC 8) 443-444, (2004), p. 123-126

[10] Winterer, M.: genfit 1.0 X MW03/22/06. 2006. – Programm zur XRD Einzelreflexanpassung mittels pseudo-Voigt Funktion, private communications

[11] Finger, L. W. ; Hazen, R. M.: Crystal structure and isothermal compression of Fe₂O₃, Cr₂O₃ and V₂O₃ to 50kbars, J Appl Phys 51 (1980) p. 5362-5367

[12] Shin, H.-S.: An Study on the Structure of Maghemite (γ -Fe₂O₃) I-Rietveld Analysis of Powder XRD Patterns-, J Korean Ceram Soc 35 (1998), No. 10, p. 1113-1119

[13] Tronc, E.; Chaneac, C.; Jolivet, J. P.: Structural and Magnetic Characterization of ϵ -Fe₂O₃, J Solid State Chem 139 (1998) p. 93-104

[14] Zboril, R.; Mashlan, M.; Petridis, D.: Iron(III) Oxides from Thermal Processes-Synthesis, Structural and Magnetic Properties, Mössbauer Spectroscopy Characterization, and Applications, Chem Mater 14 (2002) p. 969-982

[15] Granqvist, C. G.; Buhrman, R. A.: Ultrafine metal particles, J Appl Phys 47 (1976) No. 5, p. 2200-2219

[16] Kim, S. G.; Brock, J. R.: Formation of primary metal particles in evaporation chambers, J Appl Phys 60 (1986) No. 2, p. 509-513